Journal of Ceramic Processing Research. Vol. 21, No. 3, pp. 378~385 (2020)
(Received 15 December 2019, Received in revised form 19 March 2020, Accepted 20 March 2020)
https://doi.org/10.36410/jcpr.2020.21.3.378

J O U R N A L O F
Ceramic Processing Research

Impacts of praseodymium substitution on structural, spectral, magnetic and electrical properties of strontium W-type hexaferrites

Yujie Yang*, Xiansong Liu, Shuangjiu Feng, Qingrong Lv, Xucai Kan and Ruiwei Zhu
Engineering Technology Research Center of Magnetic Materials, School of Physics & Materials Science, Anhui University, Hefei 230601, P. R. China

Praseodymium substituted strontium W-type hexaferrites $Sr_{1-x}Pr_xZn_{0.8}Co_{1.2}Fe_{16}O_{27}$ ($0.00 \le x \le 0.40$) were prepared via the conventional ceramic technique. XRD analysis of W-type hexaferrites with Pr content (x) of $0.00 \le x \le 0.24$ shows the single W-type hexaferrite phase. However, for the W-type hexaferrites with Pr content (x) ≥ 0.32, the impurity phase (α-Fe_2O_3) is detected. FE-SEM images show that the grains are platelet-like shapes. The saturation magnetization (M_s), remanent magnetization (M_r) and magneton number (n_B) first increase with Pr content (x) from 0.00 to 0.16, and then decrease when Pr content (x) ≥ 0.16. The M_r/M_s ratio, magnetic anisotropy field (H_a), coercivity (H_c) and maximum energy product [$(BH)_{max}$] increase with Pr content (x) from 0.00 to 0.40. While the first anisotropy constant (K_1) increases with Pr content (x) from 0.00 to 0.16, and then decreases when Pr content (x) ≥ 0.16. The DC electrical resistivity (ρ) decreases with Pr content (x) from 0.00 to 0.40.

Keywords: W-type hexaferrites, Conventional ceramic technique, X-ray diffraction, Magnetic properties, Electrical resistivity.

Introduction

Hexagonal ferrites are playing a major role in the field of permanent magnetic materials in the market because of their low costs, high saturation magnetization, high coercivity, and perfect chemical stability [1, 2]. Hexagonal ferrites have been extensively used in microwave devices and electromagnetic wave absorbers due to their high saturation magnetization, tunable dielectric properties, high planar magnetic anisotropy, and perfect chemical stability [3]. Hexagonal ferrites are classified into six different possible types based on the chemical and crystalline structure, which include M, W, Y, X, Z and U hexaferrites, depending upon their crystal structure [4]. The strontium W-type hexaferrites ($SrMe_2Fe_{16}O_{27}$) have a crystalline structure as stacking of R (composition: $SrFe_6O_{11}$) and S (spinel block, with composition: Fe_6O_8) stocks. The main structure of W-type hexaferrites consists of SSRS*S*R*. The asterisk means that the corresponding block is rotated 180° alone the c-axis [5]. In the W-type hexaferrites, the Fe^{3+} ions are distributed among seven different crystal positions, such as four octahedral positions (12k, $4f_{VI}$, 6g, and 4f), two tetrahedral positions (4e, $4f_{IV}$), and one hexahedral position (2d) [6].

Various methods have been proposed to synthesize the W-type hexaferrites, such as the chemical co-precipitation method [7], sol-gel technique [8], sol-gel auto combustion technique [9], citrate method [10], conventional ceramic technique [11], and glass crystallization method [12]. In the present work, the conventional ceramic technique has been used to synthesize the W-type hexaferrites due to its numerous virtues, namely, simplicity, high productive and well controllable grain size as compared with other methods.

Rare earth elements (RE) have typical relaxation characteristics, which may affect the electromagnetic properties of the ferrites [13]. Ahmad et al. studied La substituted W-type hexaferrites $BaZn_2La_xFe_{16-x}O_{27}$ ($0 \le x \le 1.0$) synthesized by co-precipitation method and observed that the saturation magnetization and remanence decreased with La content (x) from 0 to 1.0, while the coercivity (H_c) increased with La content (x) from 0 to 1.0 [14]. Sadiq et al. worked on Ce-substituted W-type hexagonal ferrites $Sr_{3-x}Ce_xFe_{16}O_{27}$ ($0 \le x \le 0.10$) prepared by sol-gel method and found that with the doping of Ce^{3+} ions, the grain size decreased and the saturation magnetization and coercivity increased [15]. Xu et al. synthesized Nd^{3+} doped W-type ferrites $Ba_{1-x}Nd_xCo_2Fe_{16-x}O_{27}$ ($0.00 \le x \le 0.25$) by sol-gel method, and observed that the real part of complex permeability (ε') and imaginary part (ε'') increased with the addition of Nd^{3+} amount, while the imaginary part of complex permittivity (μ'') increased and real part (μ') went down when Nd^{3+} ions doped Ba^{2+} ions [16]. Wang et al. fabricated Sm-substituted W-type barium hexaferrites $Ba_{1-x}Sm_xCo_2Fe_{16}O_{27}$ ($0.0 \le x \le 0.2$) via conventional solid-state reaction, and found that ε' and ε'' increased slightly with Sm^{3+} ions doping and the values of μ' and

*Corresponding author:
Tel : +86 551 63861257
Fax: +86 831 63861257
E-mail: loyalty-yyj@163.com

μ″ were improved significantly when x = 0.15 [17]. Aen et al. synthesized the Ho-substituted W-type hexagonal ferrites $Ba_{1-x}Ho_xCo_2Fe_{16}O_{27}$ ($0.0 \leq x \leq 0.1$) using the sol-gel auto combustion technique, and observed that the DC electrical resistivity increased with increasing Ho^{3+} content (x) and the Ho^{3+} substitution caused the dielectric constant (real and imaginary part of complex permeability) and loss tangent to decrease [18]. Huang et al. have prepared Er^{3+}-substituted W-type barium ferrites $Ba_{1-x}Er_x(Zn_{0.3}Co_{0.7})_2Fe_{16}O_{27}$ ($0.00 \leq x \leq 0.20$) by polymer absorbent combustion and observed that all XRD patterns showed the pure phase of W-type barium ferrite when $x \leq 0.15$, while the impurity phase of $ErFeO_3$ appeared when x = 0.20; and the electromagnetic properties were significantly improved when x = 0.10 [19]. Khan et al. synthesized Ce-Mn substituted W-type hexagferrites $Sr_{1-x}Ce_xCo_2Mn_yFe_{16-y}O_{27}$ ($0.00 \leq x \leq 0.06$, $0.0 \leq y \leq 0.6$) by chemical co-precipitation method and found that the saturation magnetization, remanence, squareness ratio and coercivity increased with increasing Ce-Mn concentration up to a certain substitution level, while the room temperature resistivity decreased with increasing Ce-Mn concentration [20]. Khan et al. prepared the Nd-Ni substituted W-type hexagferrites $Sr_{1-x}Nd_xCo_2Ni_yFe_{16-y}O_{27}$ ($0.00 \leq x \leq 0.10$, $0.0 \leq y \leq 1.0$) via the chemical co-precipitation method and observed that the saturation magnetization, remanence, squareness ratio and coercivity increased with increasing Nd-Ni concentration up to a x = 0.025, y = 0.25 and then decreased continuously, the increase in magnetic properties is helpful for their applications in magnetic recording media [21].

However, the impact of praseodymium substitution on magnetic properties of strontium W-type hexaferrites has not been reported. Thus, in this work, we have fabricated praseodymium substituted strontium W-type hexaferrites $Sr_{1-x}Pr_xZn_{0.8}Co_{1.2}Fe_{16}O_{27}$ ($0.00 \leq x \leq 0.40$) by conventional ceramic technique. Effects of praseodymium substitution on the microstructural, spectral, magnetic and electrical properties of strontium W-type hexaferrites were systematically investigated for the first time.

Experimental Work

Strontium carbonate ($SrCO_3$) (99.5%), praseodymium oxide (Pr_6O_{11}) (99.9%), zinc oxide (ZnO) (99%), cobalt oxide (CoO) (99%), iron oxide (Fe_2O_3) (99.3%) were used as raw materials. All regents were used as received, i.e. no further purification of the chemicals was carried out. The praseodymium substituted strontium W-type hexaferrites $Sr_{1-x}Pr_xZn_{0.8}Co_{1.2}Fe_{16}O_{27}$ ($0.00 \leq x \leq 0.40$) were synthesized by the conventional ceramic technique. The raw materials were stoichimetrically weighed, and then ball-milled in water for 10 h in a ball mill. The ball-milled powder was dried, and pressed into pellets with a diameter of 30 mm and a thickness of 16 mm. The pellets were calcined in a muffle furnace at 1,280 °C for 3.0 h in air to obtain W-type hexaferrite phase. Subsequently, the calcined pellets were crushed by a vibration mill to obtain fine powders through a sieve with a 200 mesh. And then, the crushed magnetic powders were pressed into pellets with a diameter of 20 mm and a thickness of 8 mm. The pellets were finally sintered in a muffle furnace at 1,205 °C for 2.0 h in air, and used for the DC electrical resitivity measurement.

The phase and crystal structure of strontium W-type hexaferrites were determined from the X-ray diffraction (XRD) patterns. The X-ray diffraction patterns were recorded from a Rigaku X-ray diffractomer equipped with Cu K_α (λ = 1.5406 Å) radiation. The 2θ angles were scanned over a range between 20° and 80° with equal steps of 0.01°. Fourier transform infrared (FTIR, Nicolet 6700, Thermo Scientific) was performed to investigate the metal ion stretching and absorption bands in the wave number range of 400 to 4,000 cm^{-1}. Field emission scanning electron microscopy (FE-SEM, HITACHI S-4800) was employed to determine the grain size and morphology of strontium W-type hexaferrites. Magnetic properties were measured at room temperature using vibrating sample magnetometer (VSM) at the maximum magnetic field of 18800 Oe. DC electrical resitivity (ρ) was measured at room temperature by two probe method (Resistivity testing system, Ningbo rooko FT-353).

Results and Discussion

Fig. 1 presents the XRD patterns for strontium W-type hexaferrites $Sr_{1-x}Pr_xZn_{0.8}Co_{1.2}Fe_{16}O_{27}$ ($0.00 \leq x \leq 0.40$). XRD patterns of all samples were indexed using the standard pattern for W-type hexagonal ferrite (JCPDS card no. 75-0406). It can be observed from Fig. 1 that the W-type hexaferrites $Sr_{1-x}Pr_xZn_{0.8}Co_{1.2}Fe_{16}O_{27}$ with Pr content (x) $\leq$ 0.24 are single-phased W-type hexaferrites, while for the W-type hexaferrites $Sr_{1-x}Pr_xZn_{0.8}Co_{1.2}Fe_{16}O_{27}$ at Pr content (x) $\geq$ 0.32, the W-type hexaferrite phase is a major phase and the secondary phase α-Fe_2O_3 (JCPDS card no. 87-1166) is observed.

For W-type hexaferrites, lattice parameters *a* and *c* were obtained from the values of d_{hkl} corresponding to (1010) and (116) planes using the following equation [22]:

$$\frac{1}{d_{hkl}^2} = \frac{4}{3} \times \frac{h^2 + hk + k^2}{a^2} + \frac{l^2}{c^2}, \quad (1)$$

where d_{hkl} is the inter planner spacing in the XRD pattern, and *h*, *k* and *l* are the Miller indices. The variations of lattice parameters (*a* and *c*) for the strontium W-type hexaferrites $Sr_{1-x}Pr_xZn_{0.8}Co_{1.2}Fe_{16}O_{27}$ ($0.00 \leq x \leq 0.40$) are depicted in Fig. 2. By substituting the Sr^{2+} ions with Pr^{3+} ions, the lattice parameter *a* reflects less variation whereas the lattice parameter *c*

decreases with increasing Pr content (x) from 0.00 to 0.40. This is in agreement with the fact that the hexaferrites display constant lattice parameter *a* and changeable lattice parameter *c* [23]. For the strontium W-type hexaferrites with Pr substitution, the decrease in lattice parameter *c* is due to the difference in the ionic radii (Δr) of metal ions and the number of ionic substitutions. It is known that the ionic radii of Sr^{2+}, Pr^{3+}, Fe^{3+} and Fe^{2+} are 1.180 Å, 0.990 Å, 0.645 Å, and 0.78 Å, respectively. Substitution of Sr^{2+} (r = 1.180 Å) by Pr^{3+} (r = 0.990 Å) makes a negative difference in the ionic radii of Δr = -0.190 Å. For Pr substituted W-type hexaferrites $Sr_{1-x}Pr_xZn_{0.8}Co_{1.2}Fe_{16}O_{27}$, in order to compensate the excessive positive charges because of the substitution of Sr^{2+} by Pr^{3+}, some Fe^{3+} ions (r = 0.645 Å) convert into Fe^{2+} ions (r = 0.780 Å). This makes a positive difference in the ionic radii of Δr = +0.135 Å. The above two results exhibit that the crystal structures of strontium W-type hexaferrites are contracted after being substituted by Pr^{3+} ions and the lattice parameter *c* decreases with increasing Pr content (x).

The FT-IR spectra of strontium W-type hexaferrites were recorded in the wavenumber range of 400-4000 cm^{-1}. FT-IR spectra for strontium W-type hexaferrites $Sr_{1-x}Pr_xZn_{0.8}Co_{1.2}Fe_{16}O_{27}$ ($0.00 \le x \le 0.40$) are illustrated in Fig. 3. The absorption bands in the frequency range of 400-800 cm^{-1} are due to vibration bonds of the hexagonal ferrites [24]. The absorption band in the range 590-594 cm^{-1} is caused by the stretching vibrations of tetrahedral metal ion and oxygen bonding. And The absorption band in the range 438-440 cm^{-1} is attributed to the stretching vibrations of octahedral metal ion and oxygen bonding [25]. As seen from Fig. 3, the positions of absorption bands do not change obviously, and the normal vibration mode of tetrahedral cluster is higher

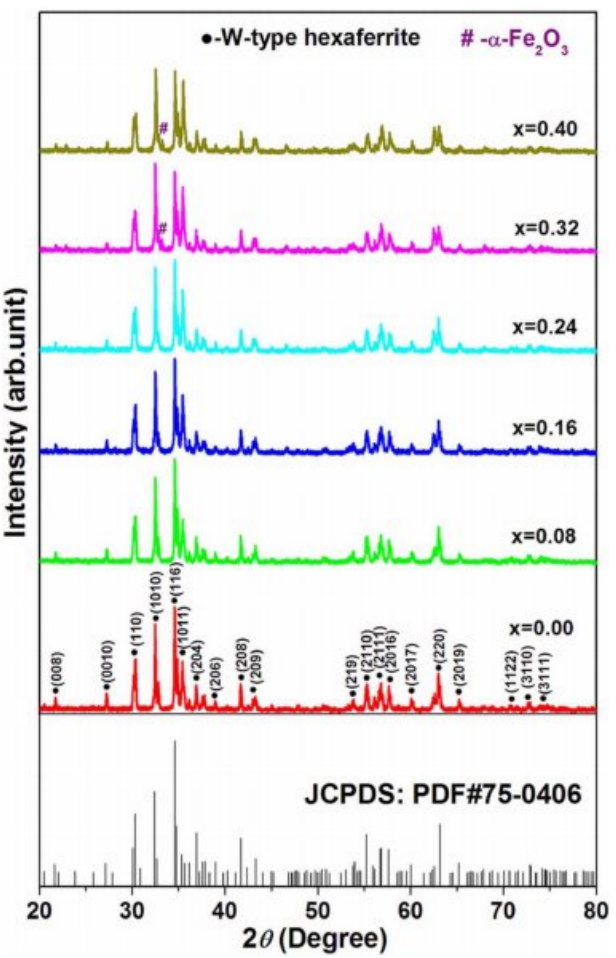

Fig. 1. XRD patterns of strontium W-type hexaferrites $Sr_{1-x}Pr_xZn_{0.8}Co_{1.2}Fe_{16}O_{27}$ ($0.00 \le x \le 0.40$).

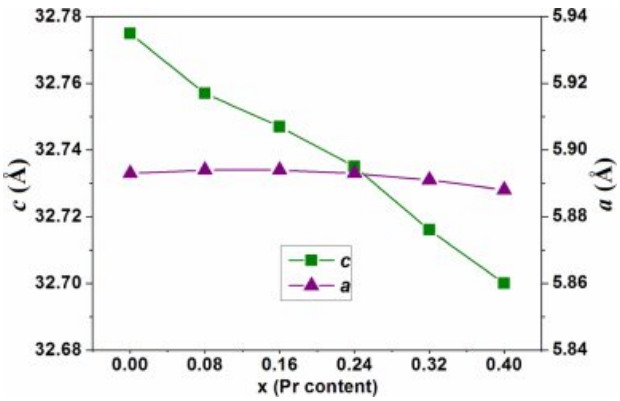

Fig. 2. Variations of lattice parameters (*c* and *a*) for strontium W-type hexaferrites $Sr_{1-x}Pr_xZn_{0.8}Co_{1.2}Fe_{16}O_{27}$ ($0.00 \le x \le 0.40$).

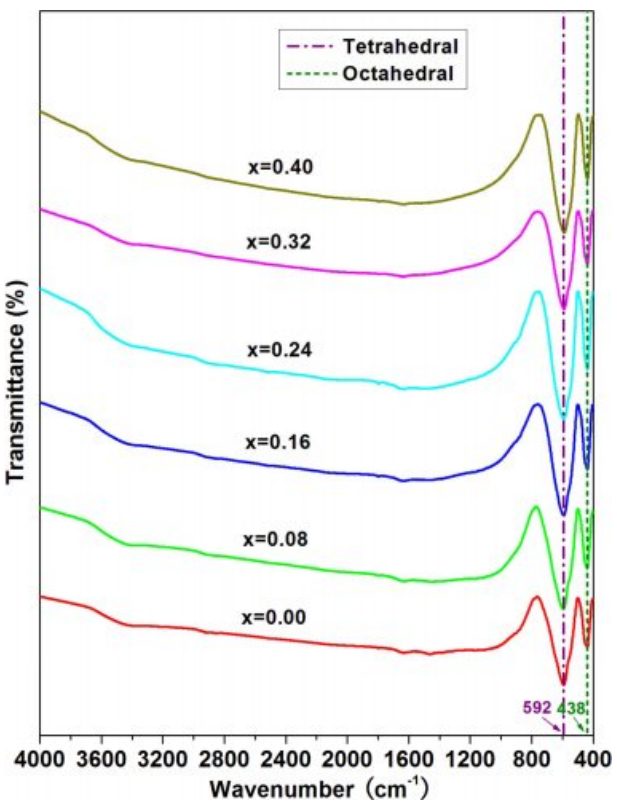

Fig. 3. FT-IR spectra for strontium W-type hexaferrites $Sr_{1-x}Pr_xZn_{0.8}Co_{1.2}Fe_{16}O_{27}$ ($0.00 \le x \le 0.40$).

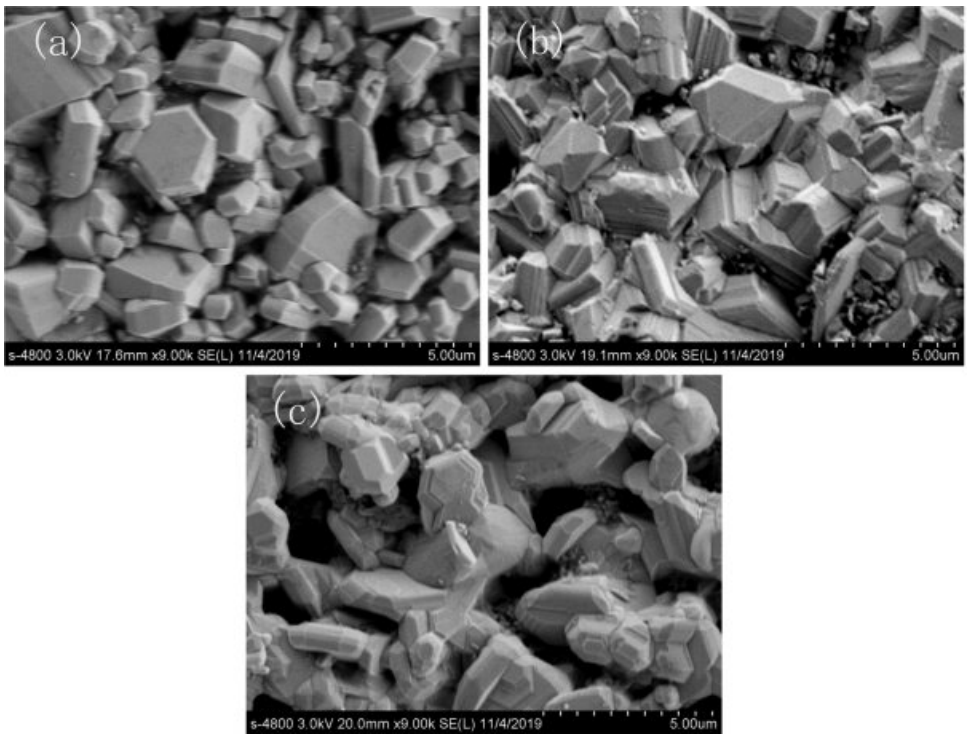

Fig. 4. FE-SEM micrographs of strontium W-type hexaferrites $Sr_{1-x}Pr_xZn_{0.8}Co_{1.2}Fe_{16}O_{27}$ with Pr content (x) of (a) x=0.00, (b) x=0.16, and (c) x=0.32.

than that of octahedral cluster. This is assigned to shorter bond length of tetrahedral cluster and longer bond length of octahedral cluster [26]. For all strontium W-type hexaferrites with different Pr content (x), the absorption band at about 1,629 cm^{-1} and about 3,389 cm^{-1} are due to the stretching vibration of surface hedroxy group (-OH) because of water in the W-type hexaferrites acquired from the process of preparation [27, 28].

Fig. 4 provides the FE-SEM micrographs of strontium W-type hexaferrites $Sr_{1-x}Pr_xZn_{0.8}Co_{1.2}Fe_{16}O_{27}$ (x=0.00, 0.16, and 0.32) under 9k magnification. It can be noted that Pr content (x) has no significant effect on the grain shape and morphology. The grains are platelet-like morphology with the average grain size of about 2.6 μm.

Magnetic hysteresis loops of strontium W-type hexaferrites $Sr_{1-x}Pr_xZn_{0.8}Co_{1.2}Fe_{16}O_{27}$ ($0.00 \leq x \leq 0.40$) are represented in Fig. 5. The values of hysteresis parameteres are calculated from magnetic hysteresis loops with different Pr content (x) and are tabulated in Table 1.

Fig. 6(a) describes the variations of saturation magnetization (M_s) and remanent magnetization (M_r) as a function of Pr content (x) for strontium W-type hexaferrites $Sr_{1-x}Pr_xZn_{0.8}Co_{1.2}Fe_{16}O_{27}$. It is observed from Fig. 6(a) that the values of M_s and M_r first increase from 68.168 and 4.528 emu/g at x = 0.00 to 78.649 and 6.292 emu/g at x = 0.16, respectively; and then decrease with Pr content (x) from 0.16 to 0.40. The magnetic moment of Fe^{3+} and Fe^{2+} ions is 5.0 μ_B and 4.0

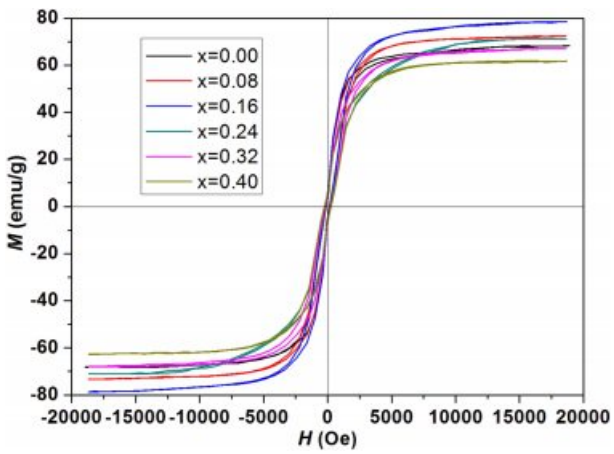

Fig. 5. Magnetic hysteresis loops of strontium W-type hexaferrites $Sr_{1-x}Pr_xZn_{0.8}Co_{1.2}Fe_{16}O_{27}$ ($0.00 \leq x \leq 0.40$).

μ_B, respectively. On the one hand, the increase in M_s and M_r with Pr content (x) from 0.00 to 0.16 can be attributed to the following reason. When Pr^{3+} ions substitute the Sr^{2+} ions in W-type hexaferrites $Sr_{1-x}Pr_xZn_{0.8}Co_{1.2}Fe_{16}O_{27}$, the shrinkage of lattice parameter *c* as shown in Fig. 2 results in the decrease of Fe-O which enhances the super-exchange interactions among the sublattices [16, 29]. Therefore, M_s and M_r are increased for the Pr substituted W-type hexaferrites ($0.00 \leq x \leq 0.16$). On the other hand, with increasing Pr content (x) from 0.16 to 0.40, the decreasing in M_s and M_r can be assignable to the below three factors. Firstly, for the hexaferrites, the Fe^{3+} ions are arranged collinearly due

Table 1. Values of the hysteresis parameteres and DC electrical resitivity (ρ) for strontium W-type hexaferrites $Sr_{1-x}Pr_x Zn_{0.8}Co_{1.2}Fe_{16}O_{27}$ ($0.00 \le x \le 0.40$).

Pr content (x)	M_s (emu/g)	M_r (emu/g)	H_c (Oe)	M_r/M_s	n_B (μ_B)	$(BH)_{max}$ (kGOe)	H_a (kOe)	ρ (10^7 ΩCm)
0.00	68.168	4.528	139.3	0.066	18.751	2.4	5.266	10.318
0.08	72.850	5.245	163.1	0.072	20.094	3.3	5.445	9.632
0.16	78.649	6.292	181.5	0.080	21.754	4.4	5.825	8.827
0.24	71.066	5.971	202.0	0.084	19.711	4.6	6.082	7.275
0.32	67.499	5.793	219.9	0.086	18.773	4.9	6.145	6.717
0.40	62.260	5.660	249.0	0.091	17.363	5.5	6.459	5.811

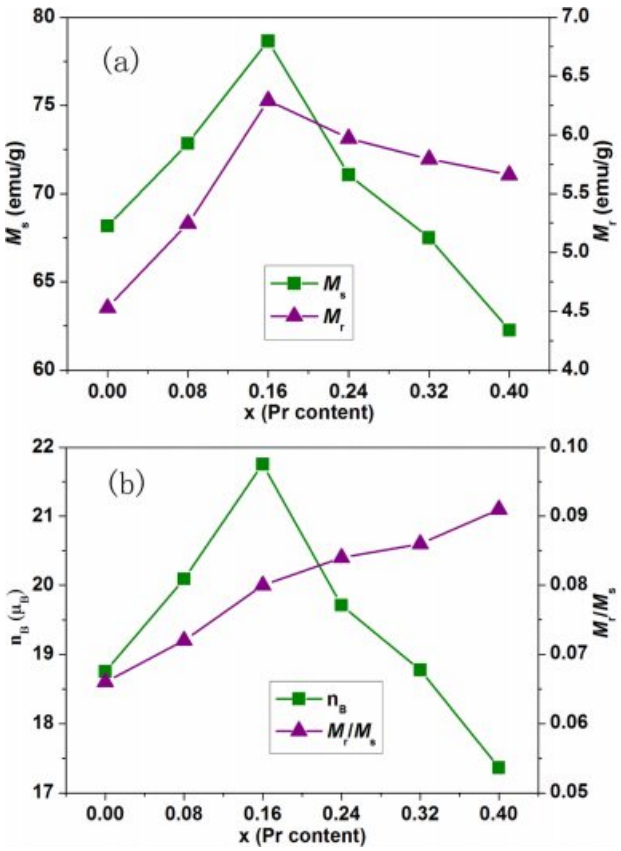

Fig. 6. Variations of (a) saturation magnetization (M_s) and remanent magnetization (M_r), and (b) magneton number (n_B) and M_r/M_s as a function of Pr content (x) for strontium W-type hexaferrites $Sr_{1-x}Pr_xZn_{0.8}Co_{1.2}Fe_{16}O_{27}$.

to the superexchange interactions. For the Pr substituted W-type hexaferrites, in order to compensate the excessive positive charges, the substitution of Sr^{2+} by Pr^{3+} causes some Fe^{3+} ions (5.0 μ_B) to convert into Fe^{2+} ions (4.0 μ_B). Abundance of Fe^{2+} ions will cause the collinearity of the superexchange interactions to break with increasing Pr content (x) from 0.16 to 0.40. This is spin canting or non-collinear magnetic order which results in the decrease of M_s and M_r [33, 34]. Secondly, the valence change of Fe^{3+} ions (5.0 μ_B) into Fe^{2+} ions (4.0 μ_B) in order to balance the excessive positive charges because of Sr^{2+} ions substituted by Pr^{3+} ions leads to the decrease of net molar magnetic moment. This is magnetic dilution [29, 30]. As a result, the values of M_s and M_r decrease continuously. Thirdly, for the W-type hexaferrites with Pr content (x) from 0.32 to 0.40, the secondary phase α-Fe_2O_3 is present as shown in Fig. 1. As a secondary phase in the W-type hexaferrites, α-Fe_2O_3 has no contribution to the increase of M_s and M_r, and can cause the values of magnetization to dilute. This leads to the decrease of M_s and M_r.

The Bohr magneton number (n_B) of strontium W-type hexaferrites with different Pr content (x) was calculated by the following relation [31]:

$$n_B = \frac{M.W. \times M_S}{5585}, \tag{2}$$

where $M.W.$ is the molecular weight and M_s is the saturation magnetization. The M_r/M_s ratio is calculated from magnetic data. The variations of magneton number (n_B) and M_r/M_s as a function of Pr content (x) for strontium W-type hexaferrites $Sr_{1-x}Pr_xZn_{0.8}Co_{1.2}Fe_{16}O_{27}$ are mentioned in Fig. 6(b). It is observed that the value of n_B increases from 18.751 μ_B at x = 0.00 to 21.754 μ_B at x = 0.16, and then decreases with increasing Pr content (x) from 0.16 to 0.40. n_B has the same varying trend as M_s exhibited in Fig. 6(a). This shows that magnetic moment is the main mechanism behind the change of M_s. The M_r/M_s ratio is known as squareness ratio. As seen from Fig. 6(b), the value of M_r/M_s ratio increases from 0.066 at x = 0.00 to 0.091 at x = 0.40. This shows that the strontium W-type hexaferrites with different Pr content (x) are multi-domain structure.

The magnetic anisotropy field (H_a) and magneto-crystalline anisotropy constant (K_1) are determined according to the law of approach to saturation [32]. The relationship between the magnetization (M) and sufficiently high magnetic fields (H) is expressed as follows [33]:

$$M = M_S\left(1 - \frac{A}{H} - \frac{B}{H^2}\right) + \chi H, \tag{3}$$

where M_s is saturation magnetization, A is a constant arising from the inhomogeneities, the constant B is related with the magnetic crystalline anisotropy constant, H is the magnetic field in this region, and χ represents

the high-field differential susceptibility. The constant A is approximate to zero. χ is neglected at high magnetic field. The M vs. $1/H^2$ plot in the high magnetic field gives a straight line. Fig. 7(a) reveals the plot of magnetization of strontium W-type hexaferrite $Sr_{0.92}Pr_{0.08}Zn_{0.8}Co_{1.2}Fe_{16}O_{27}$ as a function of $1/H^2$. The slope gives the value of B. The first anisotropy constant (K_1) can be calculated using the following equation [34]:

$$slope = -M_S B \ , \tag{4}$$

$$K_1 = M_S \left(\frac{15B}{4} \right)^{0.5} . \tag{5}$$

The calculated values of K_1 can be used to estimate the magnetic anisotropy field (H_a) of the W-type hexaferrites by using the below expression [34]:

$$H_a = \frac{2K_1}{M_S} . \tag{6}$$

The variations of H_a and K_1 as a function of Pr content (x) for strontium W-type hexaferrites $Sr_{1-x}Pr_xZn_{0.8}Co_{1.2}Fe_{16}O_{27}$ are exhibited in Fig. 7(b). It could be seen that the value of K_1 initially increases from 1.795×10^5 emu/cm^3 at x = 0.00 to 2.291×10^5 emu/cm^3 at x = 0.16, and then decreases when Pr content (x) ≥ 0.16; while the value of H_a increases from 5.266 kOe at x = 0.00 to 6.459 kOe at x = 0.40 as a result of increasing Pr content (x). The increase of H_a can ascribed to the following two reasons. Firstly, for the hexaferrites, the low symmetry of trigonal bipyramidal 2b site is the main contributor to the stronger uniaxial magnetocrystalline anisotropy [35]. Substitution of Sr^{2+} (r = 1.180 Å) by Pr^{3+} (r = 0.990 Å) can lead to greater lattice distortion and lower symmetry of trigonal bipyramidal 2b site [36]. This causes H_a to increase. Secondly, it has been reported that Fe^{2+} ions could increase the magnetic anisotropy field because of strong magnetocrystalline anisotropy of Fe^{2+} ions [37]. The number of Fe^{2+} ions increases with increasing Pr content (x) because the substitution of Sr^{2+} by Pr^{3+} causes some Fe^{3+} ions to convert into Fe^{2+} ions in order to compensate the excessive positive charges. Thus, H_a is enhanced.

Fig. 8(a) represents the variation of coercivity (H_c) as a function of Pr content (x) for strontium W-type

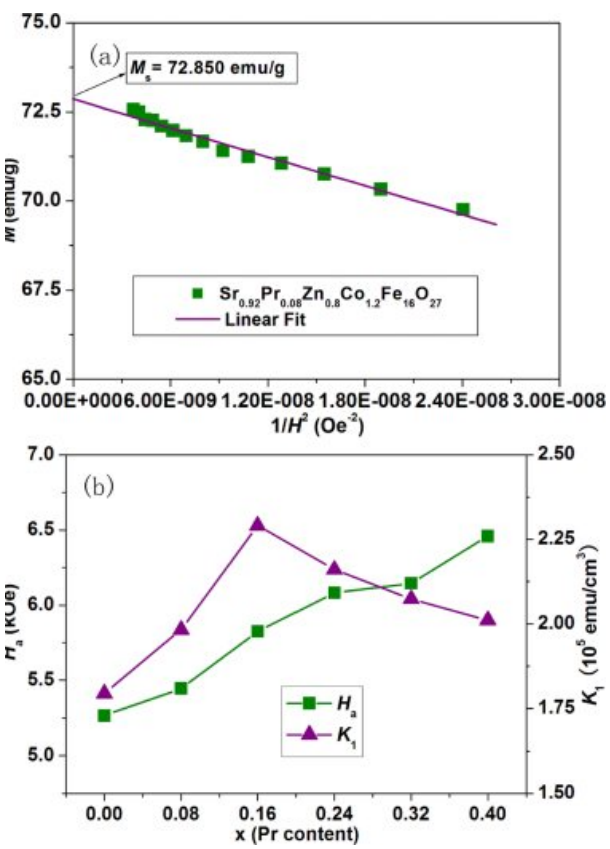

Fig. 7. (a) A plot of magnetization of strontium W-type hexaferrite $Sr_{0.92}Pr_{0.08}Zn_{0.8}Co_{1.2}Fe_{16}O_{27}$ as a function of $1/H^2$, and (b) variations of the magnetic anisotropy field (H_a) and first anisotropy constant (K_1) as a function of Pr content (x) for strontium W-type hexaferrites $Sr_{1-x}Pr_xZn_{0.8}Co_{1.2}Fe_{16}O_{27}$.

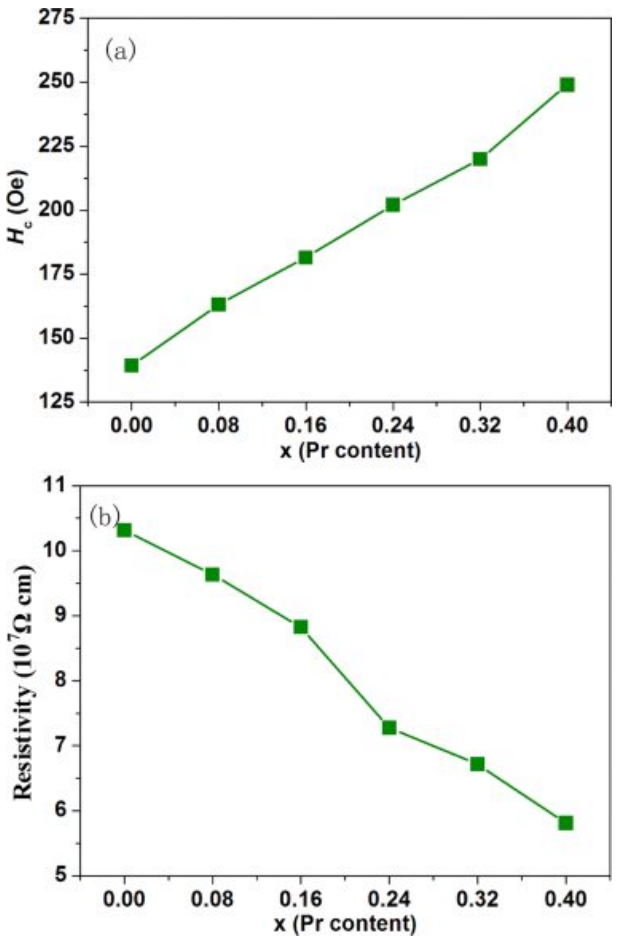

Fig. 8. Variation of (a) coercivity (H_c), and (b) DC electrical resitivity (ρ) as a function of Pr content (x) for strontium W-type hexaferrites $Sr_{1-x}Pr_x\ Zn_{0.8}Co_{1.2}Fe_{16}O_{27}$.

hexaferrites $Sr_{1-x}Pr_x$ $Zn_{0.8}Co_{1.2}Fe_{16}O_{27}$. It is worthy to note that with increasing Pr content (x), the value of H_c enhances from 139.3 Oe at x = 0.00 to 249.0 Oe at x = 0.40. The coercivity (H_c) is corrected with the intrinsic magnetic parameters and microstructure based on the following relation [38]:

$$H_c = \alpha H_a - \frac{NM_S}{\mu_0}, \quad (7)$$

where α is a microstructure factor that raises with decreasing grain size, N is called the demagnetizing factor determined by many factors one of which is aspect ratio and μ_0 is the permeability of free space. Fig. 4 shows that the platelet-like shapes and average grain size are basically unchanged with Pr substitution. Hence, α and N basically remain constant. According to the relation (7), we can conclude that the enhancement of coercivity (H_c) is primarily due to the increase of magnetic anisotropy field (H_a) as displayed in Fig. 7(b). As seen from Table 1, the value of maximum energy product [$(BH)_{max}$] for strontium W-type hexaferrites $Sr_{1-x}Pr_xZn_{0.8}Co_{1.2}Fe_{16}O_{27}$ increases with increasing Pr content (x) from 0.00 to 0.40. It is well known that the maximum energy product can be obtained by multiplying the corresponding B and H values at the point of operation on the demagnetizing curves [39]. Therefore, the values of the remanent magnetization (M_r) and coercivity (H_c) have effect on the value of $(BH)_{max}$. As seen from Fig. 6(a) and Fig. 8(a), the changing trend of $(BH)_{max}$ are owing to both the variation of M_r and variation of H_c. Therefore, magnetic properties of the strontium W-type hexaferrites can be increased with the substitution of Pr^{3+} ions for Sr^{2+} ions.

The variation of DC electrical resitivity (ρ) as a function of Pr content (x) for strontium W-type hexaferrites $Sr_{1-x}Pr_xZn_{0.8}Co_{1.2}Fe_{16}O_{27}$ is revealed in Fig. 8(b) and the values of ρ are also listed in Table 1. It can be observed that ρ is obviously affected by Pr content (x). With the increase of Pr content (x), the electrical resitivity (ρ) decreases from 10.318×10^7 Ωcm at x = 0.00 to 5.8113×10^7 Ωcm at x =0.40. It is reported that the conductivity in the hexaferrites can be attributed to the hopping between Fe^{3+} and Fe^{2+} ions at the octahedral sites [39]. For Pr substituted W-type hexaferrites $Sr_{1-x}Pr_xZn_{0.8}Co_{1.2}Fe_{16}O_{27}$, in order to compensate the excessive positive charges because of the substitution of Sr^{2+} by Pr^{3+}, some Fe^{3+} ions convert into Fe^{2+} ions. This increases the number of Fe^{2+} ions which leads to the increase of the hopping probability between the Fe^{3+} and Fe^{2+} ions. Thus, the above factors cause the electrical resitivity (ρ) to decrease.

Conclusions

The conventional ceramic technique was used to synthesize praseodymium substituted strontium W-type hexaferrites $Sr_{1-x}Pr_xZn_{0.8}Co_{1.2}Fe_{16}O_{27}$ ($0.00 \le x \le 0.40$). XRD patterns of W-type hexaferrites with Pr content (x) of $0.00 \le x \le 0.24$ show the single W-type hexaferrite phase. However, for W-type hexaferrites with Pr content (x) ≥ 0.32, the impurity phase (α-Fe_2O_3) is detected. FE-SEM images show that the grains are platelet-like shapes. M_s, M_r, and n_B first increase with Pr content (x) from 0.00 to 0.16, and then decrease when Pr content (x) ≥ 0.16. The M_r/M_s ratio, H_a, H_c and $(BH)_{max}$ increase with Pr content (x) from 0.00 to 0.40. While K_1 increases with Pr content (x) from 0.00 to 0.16, and then decreases when Pr content (x) ≥ 0.16. The DC electrical resitivity (ρ) decreases with Pr content (x) from 0.00 to 0.40.

Acknowledgements

This work was supported by the National Natural Science Foundation of China (Nos. 51872004, 5180 2002), Education Department of Anhui Province (Nos. KJ2013B293, KJ2018A0039).

References

1. L. Lechevallier, J.M. Le Breton, J.F. Wang, and I.R. Harris, J. Magn. Magn. Mater. 269[2] (2004) 192-196.
2. P. Shepherd, K.K. Mallick, and R.J. Green, J. Magn. Magn. Mater. 311[2] (2007) 683-692.
3. S.Wei, Y. Liu, H. Tian, H. Tong, Y.Liu, and B.Xu, J. Magn. Magn. Mater. 377 (2015)[1] 419-423.
4. R.C. Pullar, Prog. Mater. Sci. 57[7] (2012) 1191-1334.
5. D.M. Hemeda, A. Al-Sharif, and O.M. Hemeda, J. Magn. Magn. Mater. 315[1] (2007) L1-L7
6. X.Z. Zhou, I. Horio, A.H. Morrish, Z.W. Li, and K. Hanava, IEEE Trans. Magn. 27[6] (1991) 4651-4653.
7. M.J. Iqbal, R.A. Khan, S. Mizukami, and T. Miyazaki, J. Magn. Magn. Mater. 323[16] (2011) 2137-2144.
8. L. Deng, L. ding, K. Zhou, S. Huang, Z. Hu, and B.C. Yang, J. Magn. Magn. Mater. 323[14] (2011) 1895-1898.
9. M. Ahmad, I. Ali, F. Aen, M.U. Islam, M. N. Ashiq, S. Atiq, W. Ahmad, and M.U. Rana, Ceram. Int. 38[2] (2012) 1267-1273.
10. S. Ruan, B. Xu, H. Suo, F. Wu, S. Xiang, and M. Zhao, J. Magn. Magn. Mater. 212[1-2] (2000) 175-177.
11. F. Lv, X. Liu, S. Feng, K. Huang, X. Niu, X. Huang, F. Huang, Y. Ma, S. Jiang, and Y. Wu, Mater. Lett. 157[20] (2015) 277-280.
12. C. Sürig, K.A. Hempel, R. Müller, and P. Görnert, J. Magn. Magn. Mater. 150[2] (1995) 270-276.
13. F. Gu, G. Ji, J. Xu, H. Zou, S. Gan, and X. Xu, J. Magn. Magn. Mater. 324[6] (2012) 1209-1213.
14. M. Ahmad, F. Aen, M.U. Islam, S.B. Niazi, and M.U. Rana, Ceram. Int. 37[8] (2011) 3691-3696.
15. I. Sadiq, I. Khan, F. Aen, M.U. Islam, and M.U. Rana, Physica B 407[8] (2012) 1256-1261.
16. J. Xu, H. Zou, H. Li, G. Li, S. Gan, and G. Hong, J. Alloys Compd. 490[1-2] (2010) 552-556.
17. L.X. Wang, J. Song, Q.T. Zhang, X.G. Huang, and N.C. Xu, J. Alloys Compd. 481[1-2] (2009) 863-866.
18. F. Aen, M.F. Wasiq, M.U. Rana, H.M. Khan, and H.A. Khan, Ceram. Int. 42[14] (2016) 16077-16083.

19. X.G. Huang, J. Zhang, H.Z. Wang, S.T. Yan, L.X. Wang, and Q.T Zhang, J. Rare Earths 28[6] (2010) 940-943.
20. I. Khan, I. Sadiq, M.N. Ashiq, and M.-U.-D. Rana, J. Alloys Compd. 509[31] (2011) 8042-8046.
21. I. Khan, I. Sadiq, I. Ali, M.-U.-D. Rana, M. Najam-Ul-Haq, A. Shah, I. Shakir, and M.N. Ashiq, J. Magn. Magn. Mater. 397 (2016)[1] 6-10.
22. P. Kaur, S.B. Narang, and S. Bahel, Ceram. Int. 42[8] (2016) 9830-983.
23. M.J. Iqbal and M.N. Ashiq, Chem. Eng. J. 136[2-3] (2008) 383-389.
24. S. Güner, I.A. Auwal, A. Baykal, and H. Süzeri, J. Magn. Magn. Mater. 416 (2016) 261-268.
25. A.M. Shaikh, S.A. Jadhav, S.C. Watawe, and B.K. Chougule, Mater. Lett. 44[3-4] (2000) 192-196.
26. A. Pradeep and G. Chandrasekaran, Mater. Lett. 60[3] (2006) 371-374.
27. A. Ghasemi, Ceram. Int. 42[3] (2016) 4143-4149.
28. X. Liu, W. Zhong, S. Yang, Z. Yu, B. Gu, and Y. Du, J. Magn. Magn. Mater. 238[2-3] (2002) 207-214.
29. X.S. Liu, W. Zhong, S. Yang, Z. Yu, B.X. Gu, and Y.W. Dou, Phys. Stat. Sol. A 193[2] (2002) 314-319.
30. J. Tang, X.S. Liu, K.M. Ur Rehman, M.L. Li, C. Zhang, X.Y. Meng, H.H. Li, and C.C. Liu, J. Mater. Sci.: Mater. Electron. 28[16] (2017) 12086-12091.
31. M.G. Han, Y. Ou, W.B. Chen, and L.J. Deng, J. Alloys Compd. 474[1-2] (2009) 185-189.
32. R.E. El Shater, E.H. El-Ghazzawy, and M.K. El-Nimr, J. Alloys Compd. 739[6] (2018) 327-334.
33. Y. Yang, F.Wang, J. Shao, D. Huang, H. He, A.V. Trukhanov, and S.V. Trukhanov, J. Alloys Compd. 765[20] (2018) 616-623.
34. Z. Zhou, Z. Wang, X. Wang, X.Wang, J.Zhang, F. Dou, M. Jin, and J. Xu, J. Alloys Compd. 610[20] (2014) 264-270.
35. I. Bsoul, S.H. Mahood, A.-F. Lehlooh, and A. Al-Jamel, J. Alloys Compd. 551[4] (2013) 490-495.
36. S. Qunnunkad, Solid State Commun. 138[9] (2006) 472-475.
37. L. Peng, L.Li, X. Zhong, Y. Hu, and S. Chen, J. Magn. Magn. Mater. 428[8] (2017) 73-77.
38. K.H.J. Buschow and F.R. De Boer, in "Physics of Magnetism and Magnetic Materials" (Springer US, 2003) p.131.
39. M. El-Saadawy, J. Magn. Magn. Mater. 219[1] (2000) 69-72.